

Structures and Burning Velocity of Biomass Derived Gas Flames

C. Liu^{1,2}, B. Yan^{1,2}, G. Chen², X.S. Bai^{*1}

¹Division of Fluid Mechanics, Lund University, 221 00 Lund, Sweden

²Faculty of Environmental Science and Engineering, Tianjin University, 30072, China

Abstract

The structures and burning velocity of biomass derived gas flames were investigated using detailed chemical kinetic simulations. The studied gaseous fuels are the air-blown gasification gas, and co-firing of gasification gas with methane. The simulated burning velocities of reference fuel compositions using two widely used chemical kinetic mechanisms, GRI Mech 3.0 and the San Diego mechanism, were compared to the experimental data with reasonable agreements (with discrepancy within 7% over most of the conditions). The results show that the structures of typical gasification gas flames and co-firing flames are essentially similar to that of methane flame – chemical reactions occur in thin zones of the order of one millimeter.

Introduction

European Union (EU) in March 2007 signed up an agreement aiming to have, by year 2020, 20% of EU's overall energy consumption coming from renewable sources such as biomass, wind, hydro and solar power from a share of 8.5% in 2007 [1]. Among the different renewable energy sources, biomass energy is attractive due to its wide availability, reduction of CO₂ emission and contribution to diversification of energy supply and rural development.

Biomass derived gas (BDG) produced via gasification, pyrolysis or fermentation processes can be used to replace fossil fuels in combustion engines. BDG is typically a mixture of H₂ and CO and may contain CH₄, CO₂, H₂O, N₂ (in air-blown gasification), and other higher hydrocarbons. The specific composition of BDG depends upon the biomass sources and the processing techniques. When BDG is used in the gas turbines originally designed for natural gas, the engine efficiency is typically reduced. It stems from the gas turbine control strategies that assure the compressor operation beneath the surge line. Compressor surge is associated with the sudden drop in delivery pressure and with aerodynamic pulsation that causes mechanical damage. There are different ways to handle this problem: modification of gas turbine geometry, de-rating the mass flow and power output and co-firing with natural gas. Co-firing of BDG with natural gas can avoid some of the problems associated with de-rating and geometry modification. A feasibility study showed that with BDG of 6 MJ/Nm³ of low heating value de-rating could be avoided when co-firing BDG with 35-50% (energy basis) natural gas in the same gas turbine designed for natural gas [2].

To improve the utilization of biomass energy, it is important to develop better understanding of the BDG combustion process, and to characterize quantitatively the BDG flames, namely their structures and burning velocities. Laminar burning velocity is an important

parameter of a combustible mixture as it contains fundamental information on reactivity, diffusivity, and exothermicity. Serrano et al. [3] reported experimentally determined laminar flame burning velocities using Schlieren images for a model gasification gas with compositions of H₂, CO and N₂ in the ratio of 21%, 24% and 55% on volume basis. They found that at similar conditions the laminar burning velocity of the model gasification gas is about 45% higher than that of methane/air mixtures. Huang et al. [4] measured the laminar burning velocity of H₂, CO and N₂ in the ratio of 28%, 25% and 47% on volume basis. Hassan et al. [5] measured the laminar burning velocity of similar mixtures but with various molar ratios. These model gasification gas mixtures resemble the BDG from air-blown gasifier but the presence of CO₂ in the BDG was excluded.

In this paper we present numerical studies on the structures and laminar burning velocities of BDG mixtures produced in a demonstration plant where air-blown gasification based on a pressurized circulating fluidized bed gasifier is used [6]. Co-firing of this gasification gas with methane is also studied.

Problem Description and Simulation Methods

We consider here a gasification gas from a IGCC plant in Värnamo, Sweden. As listed in Table 1, a typical gasification gas from this plant where air-blown gasification is used based on pressurized circulating fluidized bed gasifier has the composition of about 6% methane, 19% of carbon monoxide, 12% hydrogen, 13% of carbon dioxide, and 50% nitrogen ($\alpha = 1$) [6]. The low heating value is about 4.87 MJ/kg. A second gas, model gasification gas used in the experiments of Serrano et al. [3] is also considered for validation of the present numerical methods.

Further we consider co-firing of the gasification gas with methane, which is the main component of natural gas and also the main component of upgraded biogas

* Corresponding author: xue-song.bai@energy.lth.se
Proceedings of the European Combustion Meeting 2009

from fermentation processes. As shown in Table 1, a parameter α is used to denote the mass fraction of the gasification gas in the mixture of gasification gas and methane.

Table 1. Compositions of gasification gas and co-firing with methane (Vol. %)

α	CH ₄	CO	H ₂	CO ₂	N ₂	LHV (MJ/kg)
1	5.8	19	12	13.2	50	4.87
0.8	24.6	15.2	9.6	10.6	40	10.84
0.6	43.5	11.4	7.2	7.9	30	17.88
0.4	62.3	7.6	4.8	5.3	20	26.43
0.2	81.2	3.8	2.4	2.6	10	36.97
0	100	0	0	0	0	50.02

Two chemical kinetics mechanisms are used in this study: GRI-Mech 3.0 mechanism (Smith *et al.*) [7] and the ‘‘San Diego’’ mechanism [8]. The GRI mechanism has been tested and validated extensively for methane and natural gas combustion over a wide range of pressure and temperature conditions. It contains 53 species and 325 reactions. The ‘‘San Diego’’ mechanism was developed to model the combustion of C1–C3 hydrocarbons. In this mechanism, the number of species and reactions are optimized to be minimal both to describe the systems and phenomena satisfactorily and to have minimum cost. The San Diego mechanism consists of 40 species and 175 reactions.

Numerical simulations are performed on planar one-dimensional premixed flame configurations using the Cantera simulation package which is an open-source, object-oriented software for problems involving chemical kinetics, thermodynamics, and transport processes [9].

The flame thickness can be defined as a ratio between the maximum temperature difference and the maximum temperature gradient which occurs at the point of inflection of the profile:

$$\delta_L = \frac{T_b - T_u}{(dT/dz)_{\max}}$$

where T_u is the temperature of the unburned gas, and T_b denotes the burned gas temperature. z is the coordinate normal to the flame front. $(dT/dz)_{\max}$ is the temperature gradient along the normal direction of the flame front.

Alternatively, one can also define the flame thickness as the full width at half maximum (FWHM) of temperature, and of species CH, CH₃ and CH₂O profiles to describe the detailed reaction zone structures.

Flame structures and laminar burning velocities

Figs. 1 and 2 show the distributions of temperature and species CH, CH₂O and CH₃ in the reaction zones for the methane/air flame and the gasification gas flame. Since the landfill of waste produces a mixture of methane and carbon dioxide which can be upgraded to the so-called biogas, principally methane, the structures of the biogas/air flame is the same as the methane/air

flame. As seen, the shape of temperature profile and species mass fraction profiles for the gasification gas flame and the methane/air flame are fairly similar; the methane/air flame has a temperature about 200K higher than the gasification gas flame in the post-flame zones. The peak mass fractions of CH₂O, CH₃ and CH in the gasification gas flame are about 40% lower than those in the methane/air flame. The thickness of these species in the two flames is nearly the same.

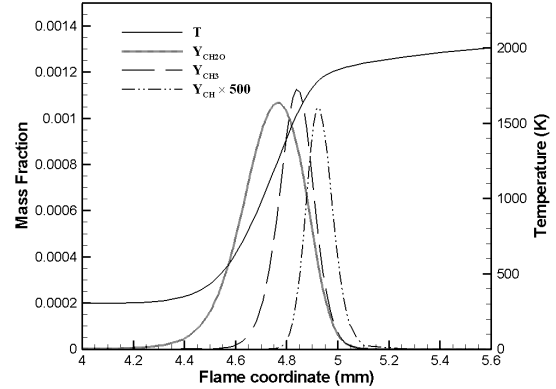


Fig.1 Compositions and temperature in a methane/air laminar flame ($\alpha = 0$) at ambient conditions, and equivalence ratio $\Phi = 1$

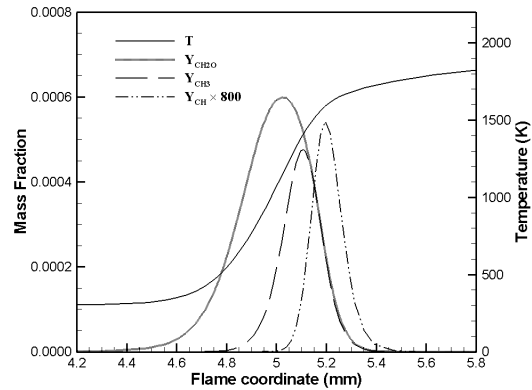


Fig. 2 Compositions and temperature for the gasification gas/air laminar flame ($\alpha = 1$) at ambient conditions, and equivalence ratio $\Phi = 1$

The laminar burning velocity of methane/air mixture has been widely studied theoretically, experimentally, and computationally. Both the GRI mechanism and the San Diego mechanism have been validated against methane/air flame experiments. Fig.3 shows the laminar burning velocity at different equivalence ratios for methane/air mixtures as well as for the co-firing mixtures. Three sets of experimental data (Law, Vagelopoulos *et al.* [10-12]) for the corresponding methane/air mixture are plotted in the figure. Both simulations and measurements indicate a maximum burning velocity around $\Phi = 1.1$ for methane/air flames at ambient conditions. This corresponds to the fact that at slightly rich conditions the flame temperature is

highest (about $\Phi = 1.07$) thereby the reaction rate is highest; in addition, the burning velocity scales with Lewis number as $s_L \sim \sqrt{Le}$. Lewis number of the mixture is higher on the rich side than on the lean side [10].

For the lean methane/air mixture over the equivalence ratio range of 0.5~1.0, the agreement between all the predictions and the measurements is reasonably good, with the San Diego mechanism predicted a slightly better result. For richer mixtures with equivalence ratio $\Phi = 1.0$ -1.6, the GRI 3.0 mechanism predicted the burning velocity in good agreement with the experiments, whereas the San Diego mechanism under-predicted the burning velocity by about 15%.

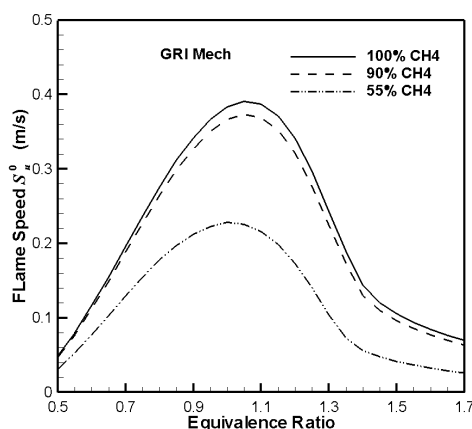
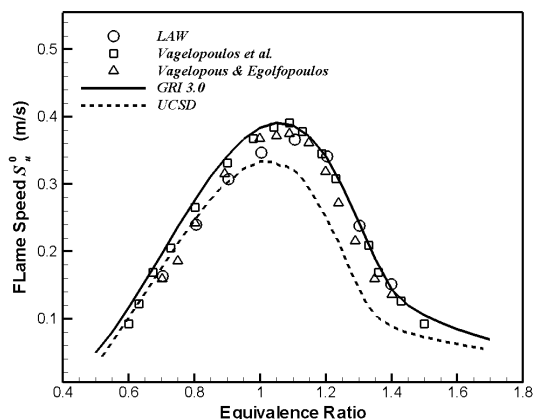


Fig. 3 Laminar burning velocity as a function of equivalence ratio for methane/air mixture (upper figure) and two landfill gas mixtures (lower figure) at ambient conditions. Symbols represent experimental data and lines are predictions by GRI 3.0 and San Diego mechanisms

For the co-firing mixtures the burning velocity profiles are essentially similar to that of the methane/air mixtures. On the lean side the burning velocity decreases rapidly as the equivalence ratio decreases, corresponding to a rapid decrease in flame temperature,

which leads the rate-ratio between the chain branching reaction $H + O_2 = O + OH$ and chain terminating reaction $H + O_2 + M = HO_2 + M$ to change in the direction in favor of the terminating reaction. Eventually, for $\Phi < 0.45$ the flame temperature is lower than the cross-over temperature (around 1200K), and the flame is quenched. On the rich side the burning velocity shows two different regimes. In the moderate rich regime ($1 < \Phi < 1.36$), the burning velocity drops rapidly as the equivalence ratio increases. In this regime the radical consumption reaction $CH_3 + H + M = CH_4 + M$ consumes H radicals rapidly as the equivalence ratio increases and thereby slow down the chain reactions and the burning velocity [13]. In the more rich regime ($\Phi > 1.36$) the fuel and oxygen co-exist in a single zone with fuel leaks to the post-flame zone, and the elementary reaction $CH_3 + CH_3 = C_2H_6$ is more dominant than radical consumption reaction $CH_3 + H + M = CH_4 + M$ [14]. This leads to a slower consumption of radical H and a slower decrease of the laminar burning velocity as the equivalence ratio increases.

It appears that the two co-firing flames have also three regimes similar to those in the methane/air flame. The difference in these flames is in the amount of methane concentration. With lower methane concentration the maximal burning velocity is shifted to $\Phi = 1$, i.e. stoichiometric condition. The profiles of the post-flame zone temperatures for the three test flames are similar, cf. Fig.4, the maximal post-flame zone temperature for all the flames are found at about $\Phi = 1.07$.

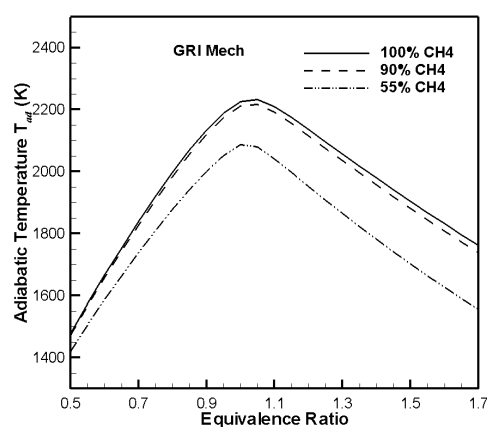


Fig. 4. Adiabatic flame temperature in the post-flame zone of methane/air flame and the co-firing flames at ambient condition

To validate the simulation for gasification gas flames, we consider the model gasification gas used by Serrano et al. [3]. The compositions of H_2 , CO and N_2 are 21%, 24% and 55% on volume basis. As shown in Fig.5, the predicted laminar burning velocities obtained using GRI and San Diego mechanisms are in reasonably good agreement with the measured data using Schlieren flame images in [3]. The laminar burning velocity is considerably higher than methane/air flame, and the

gasification gas flame from Värnamo plant. The simulations predicted a slightly higher laminar burning velocity than the experiments.

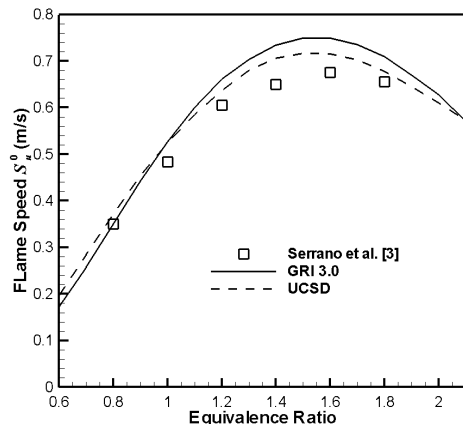


Fig. 5. Experimentally and numerically determined laminar burning velocity as a function of equivalence ratio for a model producer gas generated during the gasification of biomass wastes

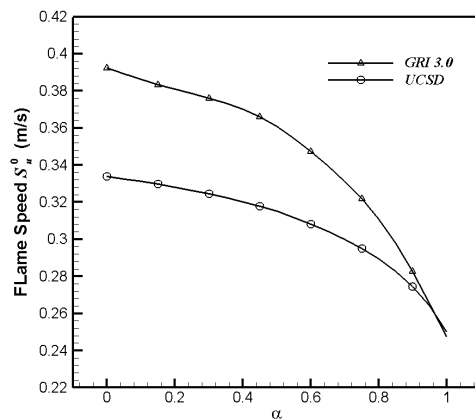


Fig. 6 Computed laminar burning velocity of co-firing flames at stoichiometric condition for different mixture ratio α

The laminar burning velocities for the co-firing gases (Table 1) at the stoichiometric condition are shown in Fig.6. It is seen that the more gasification gas in the mixture the lower the laminar burning velocities. Corresponding to this trend, the adiabatic flame temperature decreases monotonically as the fraction of the gasification gas increases, Fig.7.

Laminar flame thickness

The calculated flame thicknesses of CH_4/air flame and two co-firing flames based on the GRI mechanism for different equivalence ratios are shown in Figs.8-10. In general, the thickness defined by temperature gradient profile is the thickest, followed by the full width at half maximum of temperature, CH_2O , CH_3 , and at last CH layer is the thinnest. The thicknesses decrease as equivalence ratio increases for the lean fuel mixtures,

and reach the minimum at around stoichiometry, and then they increase again as equivalence ratio in creases for the fuel rich mixtures. The thickness of CH_3 layer is lower than the thickness of the CH_2O layer when the equivalence ratio is below about 1.5-1.6. After that, the thickness of CH_3 is higher than CH_2O . When the equivalence ratio approaches to the lean flammability limit or the rich flammability limit, the thickness of all the reaction zones becomes large before eventually quenching.

As shown in Fig.11, at the stoichiometric condition, the thickness of the gasification gas flame is less than 1 mm, and the thickness of the co-firing flames becomes thinner as the mixture ratio α decreases, i.e. the mass fraction of methane in the mixture of methane and the gasification gas increases.

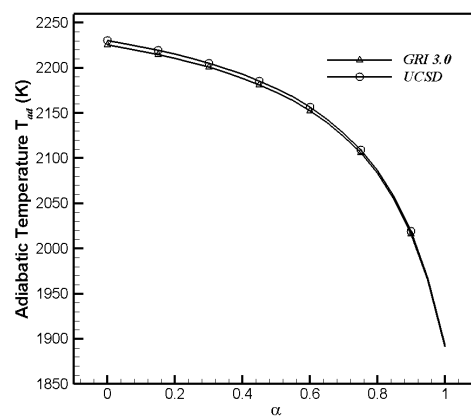


Fig. 7 Adiabatic temperature in the post-flame zones of co-firing flames at stoichiometric condition for different mixture ratio α

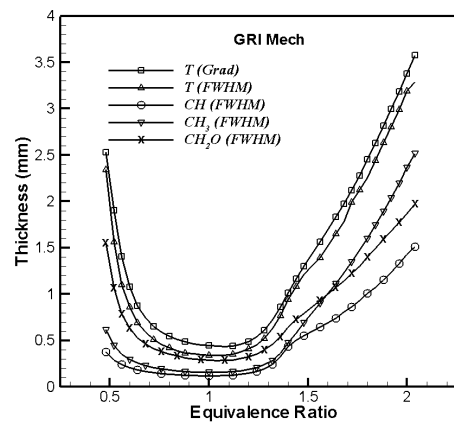


Fig. 8. Calculated flame thickness of CH_4/air flame defined by temperature gradient profile and FWHM of temperature, CH , CH_3 , CH_2O . Based on GRI 3.0 mechanism

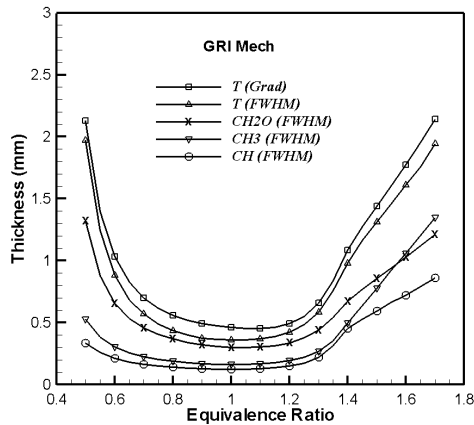


Fig. 9. Calculated flame thickness of the co-firing flame using GRI 3.0 mechanism, $\alpha = 0.1$

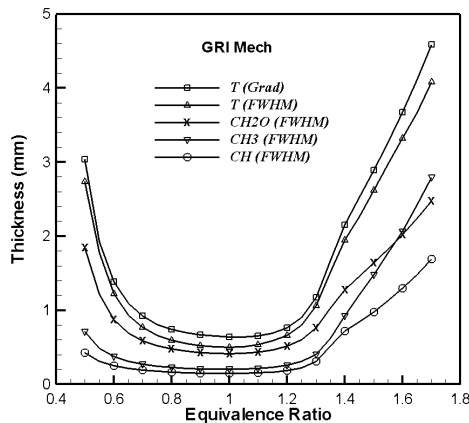


Fig. 10. Calculated flame thickness of the co-firing flame using GRI 3.0 mechanism, $\alpha = 0.45$

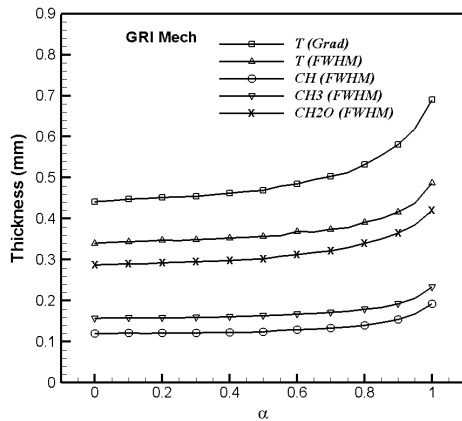


Fig. 11 The flame thickness of co-firing flames at stoichiometry at different mixture ratio α

Conclusion

The laminar burning velocity, post-flame zone temperature and the reaction zone thickness of 1-D planar freely propagating premixed flame of biomass derived gases were studied numerically. The simulated

laminar burning velocities were compared to the existing experimental data and reasonably good agreement between the simulations and experiments were found. The numerical simulations were based on two chemical kinetic mechanisms, GRI Mech 3.0 and San Diego mechanisms. The two mechanisms yield slightly different results, and this gives an estimation of data scattering from simulations. Co-firing of methane and low calorific value gasification gas was investigated. It was found that for the very low LHV gasification gases (with LHV about 5 MJ/kg) the structures of the freely propagating laminar flame is fairly similar to that of the methane/air flame. The thicknesses of the reaction zones of the gasification gas flame and co-firing flame are generally thin and on the order of methane/air flame.

Acknowledgements

This work was sponsored by the Swedish Research Council VR, SSF and STEM through CeCOST. B. Yan, C. Liu were sponsored by China Natural Science Foundation (grant no. 50428605) and CSC (China Scholarship Council).

Reference

- [1] EU renewable energy policy. <http://www.euractiv.com/en/energy/eu-renewable-energy-policy/article-117536>
- [2] J. Natarajan; T. Lieuwen; J. Seitzman, *Combustion and Flame* 2007, 151, (1-2), 104-119.
- [3] C. Serrano; J. J. Hernandez; C. Mandilas; C. G. W. Sheppard; R. Woolley, *International Journal of Hydrogen Energy* 2008, 33, (2), 851-862.
- [4] Y. Huang; C. J. Sung; J. A. Eng, *Combustion and Flame* 2004, 139, (3), 239-251.
- [5] M. I. Hassan; K. T. Aung; G. M. Faeth, *J Propul Power* 1997, 13, (2), 239-245.
- [6] K. Stahl; M. Neergaard, *Biomass and Bioenergy* 1998, 15, (3), 205-211.
- [7] G.P. Smith; D.M. Golden; M. Frenklach; N.W. Moriarty; B. Eiteneer; M. Goldenberg; C.T. Bowman; R.K. Hanson; S. Song; W.C. Gardiner Jr.; V.V. Lissianski; Z. Qin GRI 3.0. http://www.me.berkeley.edu/gri_mech/
- [8] Chemical Kinetic Mechanism for Combustion Applications, Center for Energy Research (Combustion Division), University of California at San Diego. <http://maeweb.ucsd.edu/combustion/>
- [9] <http://www.cantera.org/>, or <http://sourceforge.net/projects/cantera>, last visited 2009-01-30.
- [10] C. K. LAW, *COMBUSTION PHYSICS*. Cambridge University Press: New York, 2006.
- [11] C. M. Vagelopoulos; F. N. Egolfopoulos, *Symposium (International) on Combustion* 1998, 27, (1), 513-519.
- [12] C. M. Vagelopoulos; F. N. Egolfopoulos; C. K. Law, *Symposium (International) on Combustion* 1994, 25, (1), 1341-1347.

[13] K. Seshadri, X. S. Bai, H. Pitsch, N. Peters, Combust. Flame 113 (1998) 589-602.

[14] K. Seshadri, X. S. Bai, H. Pitsch, Combust. Flame 127 (2002) 2265-2277.